



Formation of silicon nanocomposites by annealing of $(\text{SiO}_x/\text{Sm})_n$ multilayers: luminescence, Raman and FTIR studies

Katerina V. Michailovska¹ · Ivan Z. Indutnyi¹ · Petro E. Shepeliavii¹ · Mykola V. Sopinsky¹ · Viktor A. Dan'ko¹ · Zinoviia F. Tsybrii¹ · Denys M. Maziar¹

Received: 15 January 2023 / Accepted: 29 May 2023 / Published online: 7 June 2023
© King Abdulaziz City for Science and Technology 2023

Abstract

A comparative study of the processes of metal-stimulated formation of silicon nanocrystals in SiO_x -Sm structures was carried out. Samples with identical oxide matrix stoichiometry and Sm impurity content were formed using two methods: layer-by-layer deposition and coevaporation of SiO and Sm. Studies of PL and IR absorption spectra found that the admixture of samarium in samples of both types accelerates the thermally stimulated decomposition of samarium-doped SiO_x films into Si and SiO_2 and reduces the transition temperature of silicon nanoparticles from an amorphous state to a crystalline state. However, in $(\text{SiO}_x/\text{Sm})_{10}$ multilayers, this effect is more pronounced than in single-layer films obtained using the coevaporation method. Studying the Raman spectra of $(\text{SiO}_x/\text{Sm})_{10}$ multilayers annealed at 750 °C determined that the relative volume fraction of nanocrystals in the silicon phase of the sample is ~38%. No line corresponding to the crystalline nc-Si was observed in the Raman spectra of samples deposited by co-evaporation and annealed under the same conditions. For these samples, a narrow line in the Raman spectrum corresponding to crystalline nc-Si appears only after annealing at 970 °C. In this case, the relative fraction of Si nanocrystals in the silicon phase of the sample was ~17%, 2.2 times less than for a similar multilayer annealed at 750 °C. This also indicates that, in multilayer $(\text{SiO}_x/\text{Sm})_{10}$ samples, the thermally stimulated decomposition of SiO_x , as well as the formation and crystallization of silicon nanoparticles, occurs at lower temperatures than in similar samples obtained by coevaporation. A possible mechanism for lowering the crystallization temperature of nc-Si in $(\text{SiO}_x/\text{Sm})_{10}$ multilayers is discussed.

Keywords Silicon nanoparticles · Silicon nanocomposites · Metal induced crystallization · Photoluminescence · Micro-Raman spectra · IR-spectroscopy

Introduction

Thin-film nanocomposite materials based on silicon nanoparticles (nc-Si) in an oxide matrix SiO_2 have promising potential for use in optoelectronics, photovoltaics, photonics, and microelectronics (Canham 2020; Lockwood and Pavesi 2021; Priolo et al. 2014). It is known that the efficiency of light-emitting elements based on nc-Si- SiO_2 nanocomposite materials largely depends on the size and concentration of nc-Si in the matrix (Lu et al. 1995; Zacharias et al. 2002). The deposition of suboxide SiO_x films ($0 < x < 2$) is often

used in the formation of nc-Si in an oxide matrix, followed by annealing at high temperatures (Dan'ko et al. 2005). Depending on the annealing temperature, nanosilicon structures can have different amounts of amorphous and crystalline phases, the ratio of which determines the size of silicon nanocrystals and their light-emitting characteristics. The crystallization temperature of amorphous silicon nanoparticles in a suboxide matrix is typically greater than 1000 °C and can be reduced by the presence of certain metals. For instance, the introduction of indium, which acts as a catalyst, into $\text{SiO}_{0.5}$ suboxide films can reduce the crystallization temperature of nanosilicon to 600 °C (Zamchiy et al. 2020). Tin doping of SiO_x films ($x \sim 1.15$) using thermal evaporation of a mixture of SiO_2 , Si, and Sn powders accelerates the formation of crystalline nc-Si upon thermal treatment (Voitovych et al. 2014). Study of crystallization processes showed that the temperature at which the crystallization process begins

✉ Mykola V. Sopinsky
sopinsky@ua.fm; sopinsky@isp.kiev.ua

¹ V. E. Lashkaryov Institute of Semiconductor Physics,
National Academy of Sciences of Ukraine, 41, Prosp. Nauky,
Kiev 03028, Ukraine

depends on the volume content of Sn. The a-Si crystallization mechanism proposed by the authors provided for the presence of metallic tin clusters in SiO_x , which create the conditions for an earlier transition of the amorphous silicon phase to the crystalline one (Rudenko et al. 2013). The metal-induced crystallization (MIC) method was investigated in more detail on layers of amorphous silicon (a-Si) and germanium (a-Ge) (Knaepen et al. 2009; Kryshstal et al. 2022; Neimash et al. 2013, 2015). Understanding of the MIC mechanism in various systems containing a metal–semiconductor interface (e.g. Al/a-Si, Al/a-Ge, Au/a-Si, Ag/a-Si) has been achieved as a result of theoretical studies of interface thermodynamics (Sarikov 2011; Wang et al. 2008, 2011) and experimental studies using TEM, XRD, AES (Sanwald et al. 2020; Wang et al. 2008, 2012). The MIC process is already being used for low temperature production of crystalline semiconductor films in solar cell and display technologies.

The formation of silicon nanocrystals in oxide-silicon films doped with ions of rare earth elements (lanthanides (La)) continues to be widely studied with the aim of using nc-Si as sensitizers of La^{3+} radiation. This would expand the possibility of using such materials for visible range LEDs and other optical devices (Lockwood and Pavese 2021). Structures containing erbium (Er) are the most studied, due to the fact that Er-related 1.54 μm emission corresponds to a minimum loss window of optical fiber (Franzò et al. 2003). It was found that the presence of La^{3+} (in particular, Er^{3+}) ions in a silicon oxide matrix affects the formation of silicon nanocrystals during high-temperature annealing. In particular, researchers (Mustafa et al. 2013) demonstrated the stimulating effect of Er impurity on Si nanocrystal nucleation and growth during thermal treatment of $\text{SiO}_x:\text{Er}$ films deposited by reactive sputtering. Others (Nikolenko et al. 2012; Vlasenko et al. 2012) found that air-annealing $\text{SiO}_x:\text{Er},\text{F}$ films obtained by coevaporation of SiO and ErF_3 results in more intensive crystallization of a-Si nanoparticles compared to similar annealing of evaporated SiO_x films.

Samarium-doped nanocomposites are less studied than nc-Si- $\text{SiO}_x:\text{Er}$ structures, although their promise for creating solid-state lasers, information recording, nanophosphors for display applications was demonstrated in several works (Farries et al. 1988; Kurita et al. 1994; Mbakaan et al. 2021). Therefore, in our opinion, more attention should be paid to the study of the formation processes and properties of nc-Si- SiO_x structures doped with samarium. Our earlier studies of $\text{SiO}_x:\text{Sm}$ films obtained by thermal coevaporation of SiO and metallic Sm showed that samarium impurity accelerates the local decomposition (disproportionation) of SiO_x during annealing and promotes the formation of nc-Si. Studies of the PL spectra and their dependence on the weight content of samarium, as well as Raman spectra, confirmed the presence of silicon nanocrystals in $\text{SiO}_x:\text{Sm}$ films after annealing in air at 970 °C. In SiO_x films without samarium that were

subjected to similar heat-treatment, crystalline nc-Si did not appear (Michailovska et al. 2022).

Our research sought to demonstrate the possibility of more effectively stimulating the formation of crystalline nc-Si and enhancing the luminescence properties of samarium-doped SiO_x films. For this purpose we replaced the coevaporation of SiO and Sm with sequential deposition in vacuum in the form of alternating nanolayers of SiO_x and Sm, i.e., in the form of a multilayer $(\text{SiO}_x/\text{Sm})_n$, where n is the number of pairs of SiO_x/Sm layers. Due to the island structure of Sm films of low effective thickness (< 1 nm), this made it possible to switch from a uniform spatial distribution of Sm atoms throughout the volume of SiO_x film to a cluster one. The comparative studies of the PL, IR, and Raman spectra performed in this work showed that in nanosilicon structures based on the $(\text{SiO}_x/\text{Sm})_n$ multilayer, the formation of crystalline nc-Si occurs at a lower temperature compared to the structures obtained by co-evaporation.

Experimental procedure

The investigated multilayer films $(\text{SiO}_x/\text{Sm})_n$ were obtained by alternate vacuum evaporation of SiO (Cerac Inc., Milwaukee, Wisconsin, USA, purity 99.9%) and metallic Sm powders in $\sim 10^{-3}$ Pa vacuum onto polished (111) silicon wafers and fused silica substrates. The deposited films consisted of $n = 10$ pairs of sequentially deposited SiO and Sm thin layers with a total multilayer thickness of 390 nm. The samarium content in the multilayer was determined by the mass ratio of SiO_x and Sm, which was monitored in situ by two calibrated quartz-crystal-oscillator monitor systems (KIT-1). The thickness of the resulting $(\text{SiO}_x/\text{Sm})_{10}$ structure was measured after deposition using an MII-4 microinterferometer and an LEF-3M-1 laser ellipsometer ($\lambda = 632.8$ nm). Previously, we demonstrated that films obtained by co-evaporation of SiO and Sm exhibited the highest luminescence intensity at a samarium content of ~ 1.5 wt % (Michailovska et al. 2022). Therefore, in the studied multilayer films $(\text{SiO}_x/\text{Sm})_{10}$, the content of samarium was set the same (1.5 wt%). This corresponds to the mass thickness of each samarium nanolayer equal to 0.20 nm. As with the cosputtered $\text{SiO}_x:\text{Sm}$ films, the multilayer samples were annealed in air. The annealing temperature varied from 600 to 970 °C, annealing time from 10 to 30 min. As a result, the phase decomposition of non-stoichiometric silicon oxide and the growth of silicon nanoparticles in the oxide matrix occurred. For comparative studies, some samples were annealed in vacuum. The reference SiO_x films were deposited under the same conditions.

Equipment, measurement procedures, and conditions used to measure PL, IR, and Raman spectra were identical to those described in our previous work (Michailovska

et al. 2022). The PL spectra were measured at room temperature in the wavelength range from 600 to 1100 nm using a ZMR-3 monochromator (spectral resolution ~ 1.2 nm for 10 μm slot in the investigated wavelength range) coupled to a photomultiplier (FEU-62 or FEU-51). The PL signal was excited by diode laser 405 nm radiation and recorded by a lock-in 232B nanovoltmeter referenced to the chop frequency of 110 Hz. After the excitation source, a 5 mm thick SS-8 filter with 350–500 nm transmission region was placed, which cut off the LED radiation in the 500–1500 nm range. The obtained PL spectra were corrected with regard to the spectral sensitivity of the measuring setup. Infrared transmission spectra of air-annealed SiO_x and $\text{SiO}_x:\text{Sm}$ samples on c-Si substrates were measured using a FTIR Spectrum BXII PerkinElmer spectrometer with a resolution of 4 cm^{-1} at the normal incidence. Raman spectra were excited by light from an Ar^+ laser with an excitation wavelength of 488 nm (excitation power on sample surface $\sim 1\text{ mW}$) and registered using a Horiba Jobin–Yvon T-64000 Raman spectrometer at room temperature in the spectral range $100\text{--}600\text{ cm}^{-1}$. An Olympus 50X/0.75 microscope objective was used. Spectral resolution was less than 0.15 cm^{-1} .

Results and discussion

In the luminescence spectra of $(\text{SiO}_x/\text{Sm})_{10}$ multilayers, the emission lines of samarium ions (Sm^{2+} и Sm^{3+}) in the spectral region of 600–1100 nm were absent both in the initial state after deposition and after heat treatment. The properties of the multilayer films are similar in this respect to those of coevaporated $\text{SiO}_x:\text{Sm}$ single-layer films with the same samarium weight content. This indicates that, at a given metal content, both methods of deposition followed by annealing do not lead to the formation of emitting centers in the form of Sm^{3+} and Sm^{2+} ions in the oxide matrix. However, as will be shown below, the samarium impurity in multilayer structures significantly affects the thermally stimulated formation of emitting Si nanoclusters despite the small effective thicknesses of metal sublayers.

Figure 1 shows the PL spectra of the $(\text{SiO}_x/\text{Sm})_{10}$ multilayer with 1.5 wt% Sm after annealing in air at 650 (1), 750 (2), and 850 °C (3) for 30 min. In the as-deposited samples, the PL signal was practically absent. After annealing at 650 °C, the resulting silicon nanocomposite exhibits bright luminescence with a wide emission spectrum in the 600–1050 nm region (curve 1). The complex shape of this spectrum is due to the presence of two overlapping PL bands. The maximum of the shorter wavelength band is located at 710 nm and the second PL band appears on curve 2 as a step in the region of 800–900 nm. The 710 nm band is usually associated with the luminescence of amorphous silicon nanoparticles (Rinnet et al. 2001).

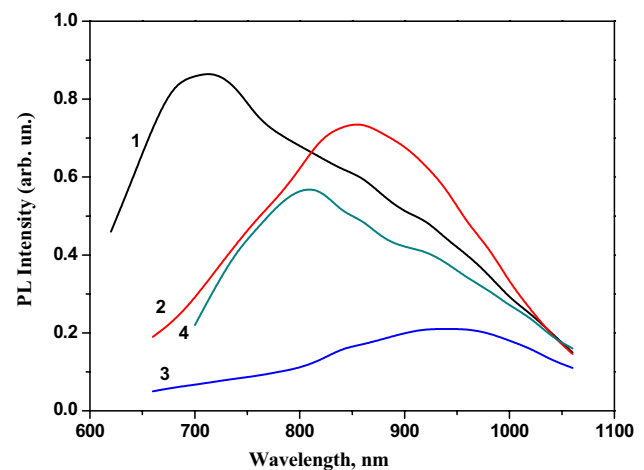


Fig. 1 Photoluminescence spectra of the $(\text{SiO}_x/\text{Sm})_{10}$ multilayers deposited on c-Si substrates after annealing them in air for 30 min at 650 (1), 750 (2), and 850 °C (3). Curve 4: PL spectrum of the $\text{SiO}_x:\text{Sm}$ coevaporated film annealed under the same conditions at 750 °C. Excitation by radiation at $\lambda = 405\text{ nm}$

After annealing at 750 °C, the PL intensity in the 710 nm band decreases significantly and the emission spectrum shifts to the long wavelength region. An intense PL band appears in the region of the step, with a maximum at 860 nm (curve 2). The 860 nm band is located in the region where the luminescence band of silicon nanocrystals formed by annealing of $\text{SiO}_{1.0}$ films at temperatures above 1000 °C is usually present (Lisovskyy et al. 2009; Kahler and Hofmeister 2002). That is, the transition of amorphous silicon clusters to the crystalline state in $(\text{SiO}_x/\text{Sm})_{10}$ multilayers is observed at a much lower temperature compared to undoped silicon suboxide films with the same stoichiometry. Our previous work showed that doping of SiO_x films with Sm, using co-evaporation of components in vacuum stimulates their decomposition into Si and SiO_2 and also reduces the transition temperature of silicon nanoparticles from an amorphous state to a crystalline state (Michailovska et al. 2022). This effect is even stronger in the $(\text{SiO}_x/\text{Sm})_{10}$ multilayers. As can be seen in Fig. 1, PL spectra of $(\text{SiO}_x/\text{Sm})_{10}$ multilayer and coevaporated $\text{SiO}_x:\text{Sm}$ single-layer films, annealed under identical conditions and of the same thickness and samarium content, are markedly different.

After annealing in air for 30 min at 750 °C, a significant part of the amorphous nanosilicon phase is still present in the film obtained using coevaporation of the components. The silicon nanoparticles that have passed into the crystalline state have a large scatter in size. This is indicated by the position of the band maximum at 800 nm and the asymmetry of its shape in the long-wavelength region of the spectrum. Previous research found that, in films obtained

by coevaporation, the PL band of crystalline nc-Si appears in the PL spectrum after annealing at higher temperatures (970 °C) (Michailovska et al. 2022). This band with a maximum at 870 nm is very close in shape and spectral composition to the band shown in Fig. 1 (curve 2). Therefore, annealing of the multilayer at 750 °C makes it possible to obtain the same concentration of silicon nanocrystals in the oxide matrix as annealing at 970 °C of a similar sample obtained by coevaporation. Such an increase in the efficiency of stimulating SiO_x decomposition and nc-Si crystallization is associated with differences in the distribution of the Sm impurity in the bulk of the film. During coevaporation, Sm and SiO_x are distributed uniformly over the film thickness, while during deposition of the multilayer, nanolayers of amorphous oxide and metal alternate. It has been demonstrated that in bilayer films consisting of a semiconductor (a-Si, a-Ge) and metal (Al, Ag), the process of metal-induced crystallization of the semiconductor begins at its interface with the metal and then the crystallization front propagates over the entire thickness of the semiconductor film (Wang et al. 2008, 2012; Sanwald et al. 2020). Similar processes also take place in SiO_x/Al ($0 < x < 2$) bilayers (Yoon 2016; Zamchiy and Baranov 2022). By analogy, it can be assumed that in the $(\text{SiO}_x/\text{Sm})_{10}$ multilayers, where there are also interphase boundaries, the crystallization of amorphous nanosilicon begins at the interfaces between Sm islands and SiO_x . As a result, the crystallization process is more efficient in comparison with films obtained by co-evaporation and even more so with undoped films. This is indicated by the appearance of an intense crystalline nc-Si band after annealing at 750 °C. In coevaporation doped films, where there are no SiO/Sm interfaces but which contain the same amount of samarium, higher annealing temperatures are required to form the same concentration of crystalline nc-Si.

As mentioned in the Introduction, the mechanism of the metal-induced crystallization in various systems containing a metal–semiconductor interface has been studied in many theoretical and experimental works (Sarikov 2011; Wang et al. 2008, 2011; Sanwald et al. 2020). For various metal–amorphous semiconductor couples, the behaviors of MICs is quite different; accordingly, various qualitative models have been proposed. In particular, the decisive role of the interface between the metal and the semiconductor in the mechanism of lowering the crystallization temperature of Si nanoparticles was established for silicon-based structures. It has been shown that a very thin interface adjacent layer of more or less mobile Si atoms is formed, which could play a decisive role in the initiation of phase transformations (crystallization). In addition, it was recognized that the phase transformation occurring at an interface can be controlled mainly by the thermodynamics of interface rather than by bulk thermodynamics. However, for the structures we studied, further studies are needed to test the assumptions

about the influence of the SiO/Sm (or Sm clusters) boundary on the samarium-induced crystallization of amorphous nanosilicon in the oxide matrix.

Increasing the annealing temperature of multilayer films to 850 °C and above leads to a decrease in the integrated radiation intensity and a shift in the band maximum from 860 to 920 nm (Fig. 1, curve 3). It is known that the photoluminescent properties of crystalline nanoparticles in a silicon oxide matrix depend on the size of nc-Si and on their volume fraction (Emelyanov et al. 2012). The observed changes in the photoluminescence of the $(\text{SiO}_x/\text{Sm})_{10}$ multilayer at high annealing temperatures ($T_{\text{an}} > 750$ °C) can be explained by the participation of samarium in the formation of crystalline nc-Si. Since samarium oxidizes very well at room temperature and above, it can be assumed that at $T_{\text{an}} > 750$ °C the Sm atoms in the silicon suboxide film more intensely interact with matrix oxygen, thereby destroying the initial Si–O bonds. This accelerates the decomposition of SiO_x and contributes to an increase in the number of nanosilicon particles and an increase in their volume fraction compared to films without samarium. Direct contact between nanoparticles can lead to their association and the formation of larger nanoclusters (Roussel et al. 2013). The decrease in the energy of the emission maximum with increasing T_{an} is apparently associated with a decrease in the quantum confinement energy for charge carriers in the formed crystalline nc-Si of a larger size. This, as well as the interaction of silicon nanoparticles with each other (the energy exchange between the nanocrystals which results in migration of excitons from nanocrystals of one size to nanocrystals of a larger size and/or to non-radiative sites in neighboring Si nanoparticles), evidently also causes a decrease in the efficiency of their luminescence.

The influence of the duration and conditions of annealing on the PL spectrum of films containing samarium was studied in order to optimize the annealing process. Figure 2 shows the PL spectra of the $(\text{SiO}_x/\text{Sm})_{10}$ multilayers after annealing in air at 750 °C for 10 (1), 20 (2), and 30 (3) min, as well as after heat treatment in vacuum at the same temperature for 30 min (4). The band at 860 nm attributed to luminescence of crystalline nc-Si appears in the PL spectrum already after 10 min of annealing (curve 1). Its intensity increases with increased annealing time, indicating an increase in the volume fraction of crystalline nc-Si and/or better passivation of their surface. In this case, the position of the band maximum, i.e., the size of crystalline nc-Si, almost does not change. The $(\text{SiO}_x/\text{Sm})_{10}$ film after vacuum heat treatment at 750 °C is characterized by a lower radiation intensity and a maximum at ~910 nm (curve 4), indicating the efficiency of annealing samples containing samarium in the presence of atmospheric oxygen. This result correlates with the results of (Chen et al. 2015) where better material quality of poly-Si thin film formed using MIC was

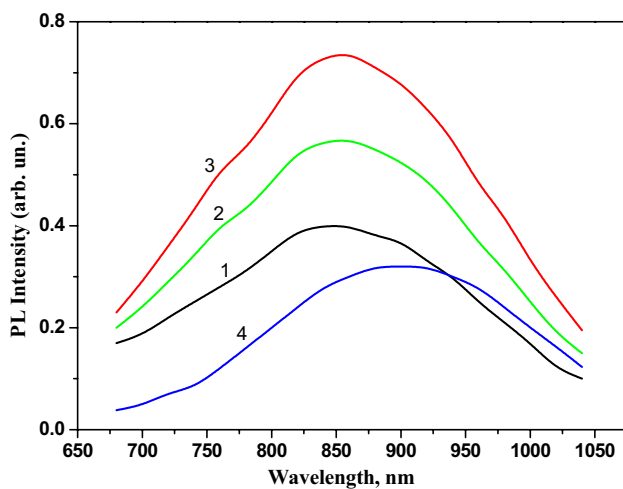


Fig. 2 Photoluminescence spectra of the $(\text{SiO}_x/\text{Sm})_{10}$ multilayers deposited on c-Si substrate after annealing in air at 750 °C for 10 (1), 20 (2), and 30 (3) min. Curve 4: PL spectrum of the same film annealed for 30 min at 750 °C in vacuum. Excitation by radiation at $\lambda = 405$ nm

obtained after annealing in oxygen atmosphere as compared to annealing in nitrogen atmosphere. In addition, partial oxidation of the formed silicon nanoparticles occurs during annealing in air (Sopinsky et al. 2015). As a result, their sizes decrease compared to similar samples annealed in vacuum or in an inert atmosphere, which leads to a short-wavelength PL shift.

The process of thermally stimulated decomposition of SiO_x into the silicon and SiO_y phases is usually written as $y\text{SiO}_x \rightarrow x\text{SiO}_y + (y-x)\text{Si}$, where x and y are the stoichiometric indices of the matrix before and after decomposition ($0 < x < y \leq 2$). The determination of these indices makes it possible to find the atomic fraction of the silicon phase ΔSi in the sample after its thermally stimulated decomposition: $\Delta\text{Si} = [(y-x)/(y(1+x))] \cdot 100\%$. IR spectroscopy is used to find the x and y indices and determine the composition of suboxide films (Dan'ko et al. 2005; Lisovskii et al. 1995). Figure 3 shows the IR transmission spectra of the $(\text{SiO}_x/\text{Sm})_{10}$ multilayer before and after annealing at 750 °C. Before annealing, the absorption maximum corresponds to the frequency $\nu_m = 993 \text{ cm}^{-1}$ (black curve), while in the annealed film, $\nu_m = 1045 \text{ cm}^{-1}$ (red curve). Using the empirical relationship between the frequency of vibrations of the bridging oxygen of the Si–O–Si bond and the value of the stoichiometry index of the oxide matrix (Nakamura et al. 1984), we found that $x = 1.04$ and $y = 1.47$. The value of the atomic fraction of the silicon phase, which precipitates in the form of nanoparticles, is $\sim 14.2\%$ ($\Delta\text{Si} = 0.142$). Due to the large atomic mass of samarium, probable incorporation of samarium atoms into the oxide matrix after annealing can lead to a slight decrease in the vibration frequency

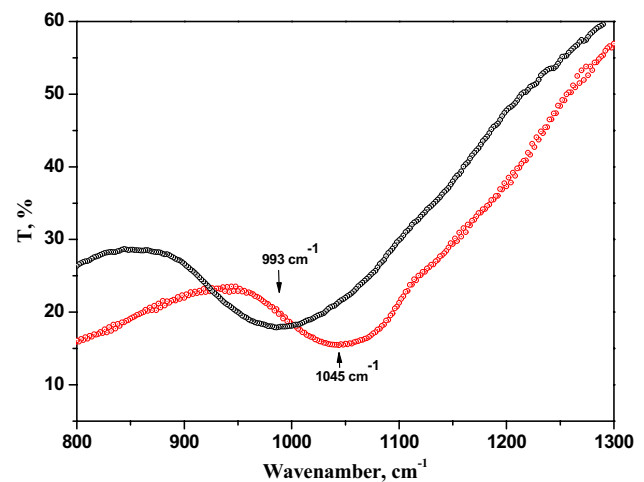


Fig. 3 IR transmission spectra of the $(\text{SiO}_x/\text{Sm})_{10}$ multilayer films deposited on a c-Si substrate (black curve) and the same film after annealing in air at 750 °C for 30 min (red curve)

of its structural units. Thus, this value is a lower estimate. Note also that the obtained value of ΔSi in the multilayer $(\text{SiO}_x/\text{Sm})_{10}$ after annealing at 750 °C is close to the value $\Delta\text{Si} = 0.15$ obtained in (Dan'ko et al. 2005) for SiO_x films annealed at 970 °C.

Raman scattering is an effective method for studying the phase composition of silicon oxide films. Figure 4 (dots) shows the Raman scattering spectrum of the $(\text{SiO}_x/\text{Sm})_{10}$ film on a fused silica substrate after its annealing in air at

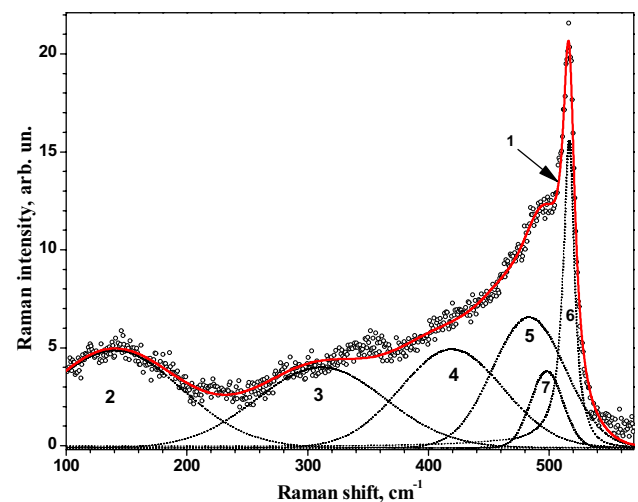


Fig. 4 Raman spectrum of the $(\text{SiO}_x/\text{Sm})_{10}$ multilayer on a fused silica substrate after annealing in air at 750 °C and its decomposition into components. Dots: experimental data. Curves 2 to 5: TA ($\sim 140 \text{ cm}^{-1}$), LA ($\sim 310 \text{ cm}^{-1}$), LO ($\sim 419 \text{ cm}^{-1}$), and TO ($\sim 483 \text{ cm}^{-1}$) bands of amorphous silicon. Curve 6: TO ($\sim 516.3 \text{ cm}^{-1}$) band of nanocrystalline silicon. Curve 7: band that can be associated with the surface of nc-Si. The red line (1) is the result of superimposition of the curves 2–7

750 °C. After decomposition of the experimental spectrum in the range of 100–570 cm^{-1} into components, we obtained the bands that are characteristic of both amorphous and crystalline nanosilicon. The bands characteristic of amorphous silicon can be attributed to transverse acoustic TA ($\sim 140 \text{ cm}^{-1}$), longitudinal acoustic LA ($\sim 310 \text{ cm}^{-1}$), longitudinal optical LO ($\sim 419 \text{ cm}^{-1}$), and transverse optical TO ($\sim 483 \text{ cm}^{-1}$) phonons. On the high-frequency side of the TO band, a narrow band with a maximum of 516.3 cm^{-1} and with a half-width $\Delta H \approx 11.1 \text{ cm}^{-1}$ is clearly visible. The appearance of the band with a maximum at $\sim 516.3 \text{ cm}^{-1}$ indicates the presence of nanocrystalline silicon in the film. The position of the maximum of the crystalline nc-Si band is shifted to the low-frequency region compared to a bulk silicon crystal due to the effect of spatial confinement of optical phonons.

To determine the relative volume fraction of nanocrystals (K_c) in the silicon phase of the studied sample ($K_c = (\text{volume of crystalline nc-Si-phase})/(\text{volume of both crystalline nc-Si and amorphous Si phases})$), we used the decomposition of the Raman spectra shown in Fig. 4 and calculated the integral intensities of the light scattering bands of the crystalline (I_c) (curve 6) and amorphous phases (I_a) (TO band, curve 5). The estimation of K_c in the silicon phase of the studied sample was carried out according to the known formula from (Voutsas et al. 1995):

$$K_c = \frac{I_c}{I_c + \sigma_0 I_a} \quad (1)$$

where σ_0 is the ratio of the integral cross sections of Raman scattering in the crystalline and amorphous phases. To determine σ_0 , an empirical dependence was used, which was obtained in the work (Bustarret et al. 1988):

$$\sigma_0 = 0.1 + \exp(-d/d_0) \quad (2)$$

where d is the average diameter of nanocrystals, d_0 —the value of the decay length of this exponential dependence, which for the excitation wavelength of an argon laser is 25 nm. Similarly to (Maslova et al. 2010), to determine the average sizes of nanocrystals, we used the relationship between d and the shift of the maximum of the Raman band of nanocrystals compared to the Raman frequency of a bulk crystal (520 cm^{-1}). (Ke et al. 2011) considered the influence of the size distribution of silicon nanocrystals on their Raman spectrum. They obtained a simple analytical expression linking the Raman frequency shift of nc-Si ($\Delta\omega$, in cm^{-1}) with their diameter (d , in nm):

$$\Delta\omega(d) = \frac{120.8}{a/d + 0.53} \times (a/d)^2 \quad (3)$$

where $a = 0.543 \text{ nm}$ is the c-Si lattice constant. Using expression (3) and the experimentally obtained value

$\Delta\omega = 520 - 516.3 \text{ cm}^{-1} = 3.7 \text{ cm}^{-1}$, we estimated the average diameter of nc-Si as $\sim 3.8 \text{ nm}$. The relative volume fraction of nanocrystals in the silicon phase of the annealed samples calculated using relations (1) and (2) was $\sim 38\%$ ($K_c = 0.38$).

Similar results were also obtained for samples deposited by coevaporation of Sm and SiO (*Fig. 5*) but only after annealing at 970 °C. Their Raman spectrum shows a narrow line at $\sim 515.3 \text{ cm}^{-1}$ with a half-width of $\Delta H \approx 12.3 \text{ cm}^{-1}$. The value of d was equal to $\sim 3.3 \text{ nm}$, close to the result for multilayer samples, while the relative fraction of Si nanocrystals, calculated using relations (1) and (2), was $\sim 17\%$ ($K_c = 0.17$). In the Raman spectrum of identical samples annealed at 750 °C under similar conditions for 30 min, no line corresponding to the crystalline nc-Si was observed. Comparison of the results of *Figs. 4* and *5* also indicates that, in multilayer samples, the thermally stimulated decomposition of SiO_x , as well as the formation and crystallization of silicon nanoparticles, occurs at lower temperatures than in similar samples (with the same stoichiometry of the oxide matrix and the same average Sm impurity content) obtained by coevaporation.

Conclusions

Comparative studies of PL spectra, IR transmission and Raman scattering of light emitting structures based on $(\text{SiO}_x/\text{Sm})_{10}$ multilayers and $\text{SiO}_x:\text{Sm}$ films, obtained by vacuum

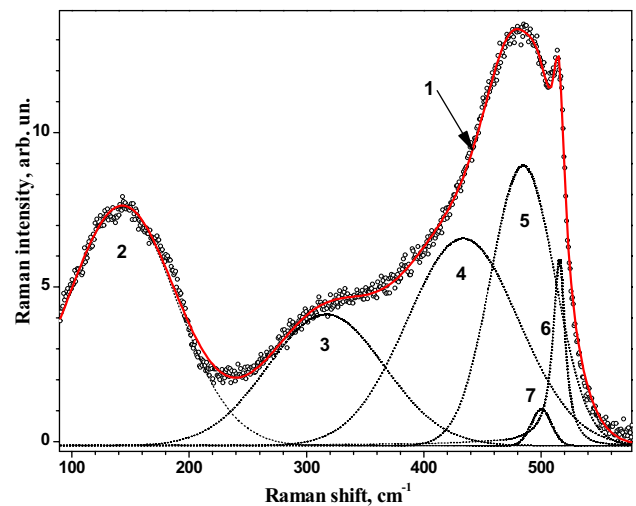


Fig. 5 Raman spectrum of a $\text{SiO}_x:\text{Sm}$ coevaporated film on a fused-silica substrate after annealing in air at 970 °C and its decomposition into components. Dots: experimental data. Curves 2–5: TA ($\sim 140 \text{ cm}^{-1}$), LA ($\sim 310 \text{ cm}^{-1}$), LO ($\sim 419 \text{ cm}^{-1}$), TO ($\sim 483 \text{ cm}^{-1}$) bands of amorphous silicon. Curve 6: TO ($\sim 516.3 \text{ cm}^{-1}$) band of nanocrystalline silicon. Curve 7: band that can be associated with the surface of nc-Si. The red line (1) is the result of superimposition of the curves 2–7

coevaporation, found that, in multilayers, the impurity of samarium more effectively accelerates the decomposition of SiO_x into Si and SiO_2 and lowers the crystallization temperature of nc-Si compared to co-evaporation samples. In particular, the relative volume fraction of nanocrystals in the silicon phase of the $(\text{SiO}_x/\text{Sm})_{10}$ multilayer annealed at 750 °C was ~38%. In similar samples, obtained by vacuum coevaporation, crystalline nc-Si begins to appear in the Raman spectrum only at 970 °C, with ~17% volume fraction of Si nanocrystals in the silicon phase only. It is assumed that the mechanism of lowering the crystallization temperature of nc-Si in multilayers is due to the presence of Sm metal clusters, analogous to metal-induced crystallization of amorphous silicon.

Acknowledgements The authors thank Jeffrey Monastyrsky (USA) for his help with the English edition of this article.

Declarations

Conflict of interest On behalf of all authors, the corresponding author states that there is no conflict of interest.

References

- Belyakov VA, Burdov VA, Lockwood R, Meldrum A (2008) Silicon nanocrystals: fundamental theory and implications for stimulated emission. *Adv Opt Technol* 208:79502. <https://doi.org/10.1155/2008/279502>
- Bustarret E, Hachicha MA, Brunel M (1988) Experimental determination of the nanocrystalline volume fraction in silicon thin films from Raman spectroscopy. *Appl Phys Lett* 52(20):1675–1677. <https://doi.org/10.1063/1.99054>
- Campbell LH, Fauchet PM (1986) The effects of microcrystal size and shape in the one phonon Raman spectra of crystalline semiconductors. *Solid State Commun* 58(10):739–741. [https://doi.org/10.1016/0038-1098\(86\)90513-2](https://doi.org/10.1016/0038-1098(86)90513-2)
- Canham L (2020) Introductory lecture: origins and applications of efficient visible photoluminescence from silicon-based nanostructures. *Faraday Discuss* 222:10–81. <https://doi.org/10.1039/D0FD00018C>
- Chen R, Zhou W, Zhang M, Wong M, Kwok HS (2015) High-performance polycrystalline silicon thin-film transistors based on metal-induced crystallization in an oxidizing atmosphere. *IEEE Electron Device Lett* 36(5):460–462. <https://doi.org/10.1109/LED.2015.2409858>
- Dan'ko VA, Indutnyi IZ, Lysenko VS, Maidanchuk IYu, Min'ko VI, Nazarov AN, Tkachenko AS, Shepelyavyy PE (2005) Kinetics of the structural and phase transformations in thin SiO_x films in the course of a rapid thermal annealing. *Semiconductors* 39(10):1197–1203. <https://doi.org/10.1134/1.2085270>
- Emelyanov AV, Shvydun AV, Zhigunov DM, Timoshenko VYu, Seminogov VN, Kashkarov PK (2012) Investigation of the dependence of the photoluminescence properties of silicon nanoclusters on their volume fraction in a silicon oxide matrix. *J Surf Investig X-Ray* 6(3):536–540. <https://doi.org/10.1134/S1027451012060092>
- Fairies MC, Morkel PR, Townsend JE (1988) Sm^{3+} -doped glass laser operating at 651 nm. *Electron Lett* 24:709–711. <https://doi.org/10.1049/el:19880479>
- Franzò G, Boninelli S, Pacifici D, Priolo F, Jacona F, Bongiorno C (2003) Sensitizing properties of amorphous Si clusters on the 1.54- μm luminescence of Er in Si-rich SiO_2 . *Appl Phys Lett* 82(22):3871–3873. <https://doi.org/10.1063/1.1579555>
- Fujii M, Yoshida M, Kanzawa Y (1997) 1.54 μm photoluminescence of Er^{3+} doped into SiO_2 films containing Si nanocrystals: evidence of energy transfer from Si nanocrystals to Er^{3+} . *Appl Phys Lett* 71(9):1198–1200. <https://doi.org/10.1063/1.119624>
- Gestel D, Gordon I, Poortmans J (2013) Aluminum-induced crystallization for thin-film polycrystalline silicon solar cells: Achievements and perspective. *Sol Energy Mater Sol Cells* 119:261–270. <https://doi.org/10.1016/j.solmat.2013.08.014>
- Kahler U, Hofmeister H (2002) Size evolution and photoluminescence of silicon nanocrystallites in evaporated SiO_x thin films upon thermal processing. *Appl Phys A* 74(1):13–17. <https://doi.org/10.1007/s003390100993>
- Ke W, Feng Y, Huang Y (2011) The effect of Si-nanocrystal size distribution on Raman spectrum. *J Appl Phys* 109(8):083526. <https://doi.org/10.1063/1.3569888>
- Knaepen W, Gaudet S, Detavernier C, Van Meirhaegle RL, Sweet J, Lavoie C (2009) In situ x-ray diffraction study of metal induced crystallization of amorphous germanium. *J App Phys* 105(8):083532. <https://doi.org/10.1063/1.3110722>
- Kryshal A, Bogatyrenko S, Ferreira P (2022) Metal-induced crystallization of amorphous semiconductor films: nucleation phenomena in Ag-Ge films. *Appl Surf Sci* 606:154873. <https://doi.org/10.1016/j.apsusc.2022.154873>
- Kurita A, Kushida T, Izumitani T, Matsukawa M (1994) Room-temperature persistent spectral hole burning in Sm^{2+} -doped fluoride glasses. *Opt Lett* 19:314–316. <https://doi.org/10.1364/OL.19.000314>
- Lisovskii IP, Litovchenko VG, Losinskii VG, Frolov SI, Flietner H, Fussel W, Schmidt EG (1995) IR study of short-range and local order in SiO_2 and SiO_x films. *J Non-Cryst Solids* 187:91–95. [https://doi.org/10.1016/0022-3093\(95\)00118-2](https://doi.org/10.1016/0022-3093(95)00118-2)
- Lisovskyy IP, Voitovich MV, Sarikov AV, Litovchenko VG, Romanyuk AB, Melnyk VP, Khatsevich IM, Shepeliavyy PE (2009) Transformation of the structure of silicon oxide during the formation of Si nano-inclusions under thermal annealing. *Ukr J Phys* 54(4):383–390
- Lockwood DJ, Pavesi L (2021) Silicon photonics IV: innovative Frontiers, vol 139. Topics in applied physics. Springer, Berlin. <https://doi.org/10.1007/978-3-030-68222-4>
- Lu ZH, Lockwood DJ, Baribeau JM (1995) Quantum confinement and light emission in SiO_2/Si superlattices. *Nature* 378(6554):258–260. <https://doi.org/10.1038/378258a0>
- Maslova NE, Antonovsky AA, Zhigunov DM, Timoshenko VYu, Glebov VN, Seminogov VN (2010) Investigation of silicon nanocrystals in silicon suboxide layers by Raman scattering spectroscopy. *Semiconductors* 44(8):1040–1043. <https://doi.org/10.1134/S1063782610080154>
- Mbakaan C, Ahemen I, Dejene FB, Onojah AD, Motloun SJ, Ocaya R, Reyes-Rojas A (2021) Structural and optical properties of nano- SiO_2 derived from the husk of some rice varieties and the effect of doping with Sm^{3+} ions. *Opt Mater Express* 11:965–987. <https://doi.org/10.1364/OME.419552>
- Michailovska KV, Indutnyi IZ, Shepeliavyy PE, Sopinskyy MV, Dan'ko VA, Tsybrii ZF, Nikolenko AS (2022) Samarium-induced enhancement of SiO_x decomposition and Si nanocrystals formation. *Appl Nanosci*. <https://doi.org/10.1007/s13204-022-02617-0>
- Mustafa D, Biggemann D, Martens JA, Kirschhock ChEA, Tessler LR, Breynaert E (2013) Erbium enhanced formation and growth of photoluminescent Er/Si nanocrystals. *Thin Solid Films* 536:196–201. <https://doi.org/10.1016/j.tsf.2013.03.027>
- Nakamura M, Mochizuki V, Usami K, Itoh Y, Nozaki T (1984) Infrared absorption spectra and compositions of evaporated silicon oxides

- (SiO_x). *Solid State Commun* 50(12):1079–1081. [https://doi.org/10.1016/0038-1098\(84\)90292-8](https://doi.org/10.1016/0038-1098(84)90292-8)
- Neimash V, Poroshin V, Shepeliavyi P, Yukhymchuk V, Melnyk V, Kuzmich A, Makara V, Goushcha AO (2013) Tin induced a-Si crystallization in thin films of Si-Sn alloys. *J Appl Phys* 114(21):213104. <https://doi.org/10.1063/1.4837661>
- Neimash VB, Goushcha AO, Shepeliavyi PE, Yuhymchuk VO, Melnyk VV, Danko VA, Kuzmich AG (2015) Self-sustained cyclic tin induced crystallization of amorphous silicon. *J Mater Res* 30(20):3116–3124. <https://doi.org/10.1557/jmr.2015.251>
- Nikolenko AS, Sopinskyy MV, Strelchuk VV, Veligura LI, Gomonovych VV (2012) Raman study of Si nanoparticles formation in the annealed SiO_x and SiO_x-Er, F films on sapphire substrate. *J Optoelectron Adv Mater* 14(1–2):120–124
- Priolo F, Gregorkiewicz T, Galli M, Krauss TF (2014) Silicon nanostructures for photonics and photovoltaics. *Nat Nanotechnol* 9(19):19–32. <https://doi.org/10.1038/nnano.2013.271>
- Rinnet H, Vergant M, Burneau A (2001) Evidence of light-emitting amorphous silicon clusters in a silicon oxide matrix. *J Appl Phys* 89(1):237–243. <https://doi.org/10.1063/1.1330557>
- Roussel M, Talbot E, Pareige P, Gourbilleau F (2013) Influence of the supersaturation on Si diffusion and growth of Si nanoparticles in silicon-rich silica. *J Appl Phys* 113(6):063519. <https://doi.org/10.1063/1.4792218>
- Rudenko RM, Voitovych VV, Kras'ko MM, Kolosyuk AG, Kraichynskiy AM, Yuchimchuk VO, Makara VA (2013) Influence of high temperature annealing on the structure and the intrinsic absorption edge of thin-film silicon doped with tin. *Ukr J Phys* 58(8):769–772. <https://doi.org/10.15407/ujpe58.08.0769>
- Sanwald P, Wang Z, Mittemeijer EJ (2020) Metal-alloy induced crystallization of amorphous silicon. *J Appl Phys* 128(4):045311. <https://doi.org/10.1063/5.0004965>
- Sarikov A (2011) Metal induced crystallization mechanism of the metal catalyzed growth of silicon wire-like crystals. *Appl Phys Lett* 99:143102. <https://doi.org/10.1063/1.3644981>
- Sopinskyy MV, Vlasenko NA, Lisovskyy IP, Zlobin SO, Tsybrii ZF, Veligura LI (2015) Formation of nanocomposites by oxidizing annealing of SiO_x and SiO_x<Er, F> films: ellipsometry and FTIR analysis. *Nanoscale Res Lett* 10:232. <https://doi.org/10.1186/s11671-015-0933-0>
- Vlasenko NA, Sopinskii NV, Gule EG, Strelchuk VV, Oleksenko PF, Veligura LI, Nikolenko AS, Mukhlyo MA (2012) Effect of erbium fluoride doping on the photoluminescence of SiO_x films. *Semiconductors* 46(3):323–329. <https://doi.org/10.1134/S1063782612030232>
- Voitovych VV, Rudenko RM, Kolosiuk AG, Krasko MM, Yuchimchuk VO, Voitovych MV, Ponomarov SS, Kraitchinskii AM, Povarchuk VYu, Makara VA (2014) Effect of tin on the processes of silicon-nanocrystal formation in amorphous SiO_x thin-film matrices. *Semiconductors* 48(1):73–76. <https://doi.org/10.1134/S1063782614010242>
- Voutsas AT, Hatalis MK, Boyce J, Chiang A (1995) Raman spectroscopy of amorphous and microcrystalline silicon films deposited by low-pressure chemical vapor deposition. *J Appl Phys* 78(12):6999–7006. <https://doi.org/10.1063/1.360468>
- Wang ZM, Wang JY, Jeurgens LPH, Mittemeijer EJ (2008) Thermodynamics and mechanism of metal-induced crystallization in immiscible alloy systems: experiments and calculations on Al/a-Ge and Al/a-Si bilayers. *Phys Rev B* 77:045424. <https://doi.org/10.1103/PhysRevB.77.045424>
- Wang ZM, Gu L, Phillipp F, Wang JY, Jeurgens LPH, Mittemeijer EJ (2011) Metal-catalyzed growth of semiconductor nanostructures without solubility and diffusivity constraints. *Adv Mater* 23(7):854–859. <https://doi.org/10.1002/adma.201002997>
- Wang ZM, Gu L, Jeurgens LPH, Phillipp F, Mittemeijer EJ (2012) Real-time visualization of convective transportation of solid materials at nanoscale. *Nano Lett* 12(12):6126–6132. <https://doi.org/10.1021/nl303801u>
- Yoon JH (2016) Fabrication of polycrystalline silicon films by Al-induced crystallization of silicon-rich oxide films. *Phys Status Solidi RRL* 10(9):668–672. <https://doi.org/10.1002/pssr.201601918>
- Zacharias Z, Heitmann J, Scholz R, Kahler U, Schmidt M, Blasing J (2002) Size-controlled highly luminescent silicon nanocrystals: a SiO/SiO₂ superlattice approach. *Appl Phys Lett* 80(4):661–667. <https://doi.org/10.1063/1.1433906>
- Zamchiy A, Baranov E (2022) Polycrystalline silicon thin films for solar cells via metal-induced layer exchange crystallization. *Coatings* 12(12):1926. <https://doi.org/10.3390/coatings12121926>
- Zamchiy AO, Baranov EA, Merkulova IE, Lunev NA, Volodin VA, Maximovskiy EA (2020) Indium-induced crystallization of silicon suboxide thin amorphous films. *Tech Phys Lett* 46(12):583–586. <https://doi.org/10.1134/S1063785020060280>

Publisher's Note Springer Nature remains neutral with regard to jurisdictional claims in published maps and institutional affiliations.

Springer Nature or its licensor (e.g. a society or other partner) holds exclusive rights to this article under a publishing agreement with the author(s) or other rightsholder(s); author self-archiving of the accepted manuscript version of this article is solely governed by the terms of such publishing agreement and applicable law.